Global and Regional Scale Precipitation Patterns Associated with the El Niño/Southern Oscillation

C. F. ROPELEWSKI AND M. S. HALPERT

Climate Analysis Center/National Meteorological Center, NWS/NOAA, Washington, DC 20233

(Manuscript received 29 August 1986, in final form 16 January 1987)

ABSTRACT

We investigate the "typical" global and large-scale regional precipitation patterns that are associated with the El Niño/Southern Oscillation (ENSO). Monthly precipitation time series from over 1700 stations are analyzed using an empirical method designed to identify regions of the globe that have precipitation variations associated with ENSO. Montly mean ranked precipitation composites are computed over idealized 2-year ENSO episodes for all stations that include data for at least five ENSOs. The amplitude and phase of the first harmonic fitted to the 24-month composite values are plotted in the form of a vector for each station. When plotted on a global map, these vectors reveal both the regions of spatially coherent ENSO-related precipitation and the phase of this signal in relation to the evolution of the composite episode. Time series of precipitation for the coherent regions identified in the harmonic vector map are examined to determine the magnitudes of the ENSO-related precipitation and the percentages of the time the identified relationship actually occurred in conjunction with ENSO episodes.

This study expands previous results by placing the regional precipitation relationships into a global framework and by providing a consistent methodology for the definition of the geographical regions and the temporal phase of ENSO-related precipitation. In addition to the Pacific Ocean basin where precipitation patterns could be directly related to the ENSO, several other regions, which showed consistent ENSO-related precipitation, were identified. Specifically, four regions in Australia, two regions each in North America, South America, the Indian subcontinent, and Africa, and one region in Central America were all found to have coherent ENSO-related precipitation. In most of these regions, the "season" of ENSO-related precipitation was found to be in phase with the normal annual precipitation cycle. Time series of area-averaged precipitation for the appropriate "seasons" show departures consistent with the composites occurring for at least 80% of the ENSO events in almost every region. The analysis further indicates that variations in precipitation related to ENSO occur as early as April of the composite episode through May of the following year.

1. Introduction

The links between the El Niño–Southern Oscillation (ENSO) and large scale precipitation patterns have been examined since the earliest studies of this phenomenon. Indeed, the pioneering studies by Walker (1923, 1924, 1928) and Walker and Bliss (1930, 1932, 1937), which first documented ENSO on a global scale, were motivated by attempts to understand and predict variations in Indian monsoon rainfall and then were expanded to studies of precipitation around the globe. Since publication of these early works, several other studies have found evidence of precipitation–ENSO relationships. Berlage (1966) found evidence of significant correlations between indices of the Southern Oscillation and precipitation at several individual stations around the globe. Stoeckenius (1981) documented significant correlations between the annual-averaged Easter Island–Darwin, Australia Southern Oscillation index and area-averaged precipitation for several areas in the tropics. Rasmusson and Wallace (1983) showed relationships between time series of rainfall at several locations and the surface pressure at Tahiti and Darwin. In other, more regionally focused studies, Rasmusson and Carpenter (1983) and Shukla and Paolino (1983) confirmed that the summer monsoon precipitation over peninsular India is suppressed during ENSO years. Horel and Wallace (1981) documented increases in precipitation over islands in the central equatorial Pacific during ENSO years. Hastenrath (1978) and Kousky et al. (1984) found relationships between ENSO and precipitation in parts of Brazil. Douglas and Englehart (1981) and, more recently, Ropelewski and Halpert (1986) found that ENSO is related to enhanced winter season precipitation in the southeastern United States. Most of these and other related previous studies presented correlations between various indices of ENSO and precipitation, or they examined monthly or seasonal precipitation time series at selected stations or regions in comparison to time series of ENSO indices.

The purpose of this paper is to provide an improved description of the typical geographical extent, magnitude, phase and duration of ENSO-related precipitation at each of several locations over the globe. We are particularly interested in identifying regions of the globe

that have relatively strong, consistent ENSO-related precipitation signals.

The data are described in section 2. The analyses of the global precipitation patterns are presented in section 3. The regional analyses are described and discussed in section 4.

TABLE 1. List of the 26 ENSO episodes included in this study. (After Rasmusson and Carpenter, 1983)

Years 1877, 1880, 1884, 1887, 1891, 1896, 1899, 1902, 1905, 1911, 1914, 1918, 1923, 1925, 1930, 1932, 1939, 1941, 1951, 1953, 1957, 1965, 1969, 1971, 1976, 1982*.

* Used in the time series plots only.

2. Data

Monthly precipitation totals for over 1700 stations around the globe provide the primary source of data in this study. The longest time series extend from 1875 to 1983 (154 stations) and span 25 ENSO episodes. Almost a third (548) of the stations contain precipitation data from the turn of the century and thus span 18 ENSO episodes. The primary source of these data is the National Center for Atmospheric Research (NCAR) World Monthly Surface Station Climatology. Most of the data are from first-order meteorological reporting stations, but precipitation data for Africa have been supplemented with observations from several hundred stations which were assembled by Nicholson (1979) and provided to NCAR. Data for many of these African stations extend from the turn of the century to the mid-1970s, thus providing a long database for the analysis. The Australian precipitation data have also been supplemented by several dozen long-period stations provided by the Australian National Climate Center. Time series of key individual stations were examined in order to remove stations with apparent biases or errors from the analysis.

3. Global precipitation relationships

The analysis methods are described in detail in Ropelewski and Halpert (1986) and are outlined below. In the first part of this analysis, we follow a suggestion of Meisner (1976) to represent the monthly precipitation data at each station as percentile ranks. For each month, the entire n-year record of precipitation data is ranked from 1, for the smallest precipitation amount, to n for the largest precipitation amount. These ranked precipitation amounts are then normalized by the number of years of record and multiplied by 100. The resulting percentile ranks place station precipitation anomalies that have differing means and variances on an equal footing and thus facilitate the interpretation of precipitation patterns in regimes that have large station-to-station differences in these statistics.

In areas of the world that have a pronounced dry season and in desert areas the time series of precipitation contain several occurrences of "zero" monthly precipitation amounts. The zero amounts represent "ties" in the ranking scheme described above. In this study the first zero precipitation amount is assigned a rank of "1", the next zero occurrence a rank of "2", and so on. Thus, in records which have a large number of zeros the ranking analysis presented here introduces a bias by ranking the most recent zero values higher than those occurring earlier in the record. We experienced difficulty with a large number of zeros in time series only in northern Africa and the Middle East.

For each station, ENSO composites of the percentile ranked precipitation are formed for the 24-month period starting with the July preceding the episode, designated Jul(−), and continuing through the June following the episode, designated Jun(+). Thus, for the 1976 ENSO episode, the period of interest runs from July 1975 to June 1977. The ENSO "years" used as the basis for the composite analysis (Table 1) are those defined in Rasmusson and Carpenter (1983). Although as many as 25 ENSO episodes are included in the composites, harmonics were computed for stations whose data span as few as 5 ENSO episodes. Data for the 1982/83 ENSO were not included in the composites to insure that this extremely strong episode did not overwhelm the results. The composite for each station is fitted with the first harmonic of an idealized 24-month ENSO cycle. The analysis is confined to only the first harmonic under the assumption that only one extreme in precipitation is associated with the ENSO extreme of the Southern Oscillation. In this idealized ENSO cycle we assume simple ENSO-precipitation relationships with one strong positive or negative precipitation anomaly over the 24-month period. If the evolution of the ENSO episode is typically related to more than one precipitation maximum or minimum, then that relationship will not be clearly identified by this analysis technique. A 24-month period was chosen to coincide with the longest unambiguous period consistent with the ENSO life time suggested in the Rasmusson and Carpenter (1982) composites. Although the Quasi-Biennial Oscillation (QBO) also has a period of near 24 months, there is little danger that the analysis will be confounded by the QBO since ENSO and the QBO are virtually uncorrelated (Quiroz, 1983a). The first harmonic (amplitude and phase) of the composite precipitation at each station is represented as a vector and plotted in Fig. 1. The plotting convention is analogous to that presented in the analysis of the annual precipitation cycle by Hsu and Wallace (1976). In the analysis convention chosen here, the phase of the vector is identified with the positive part of the cycle, i.e., more than normal precipitation. It is only through the analysis of composites, described below, that we are able to determine if the positive or negative phase, above or below normal precipitation, contains the important ENSO-related signal. The study is concerned

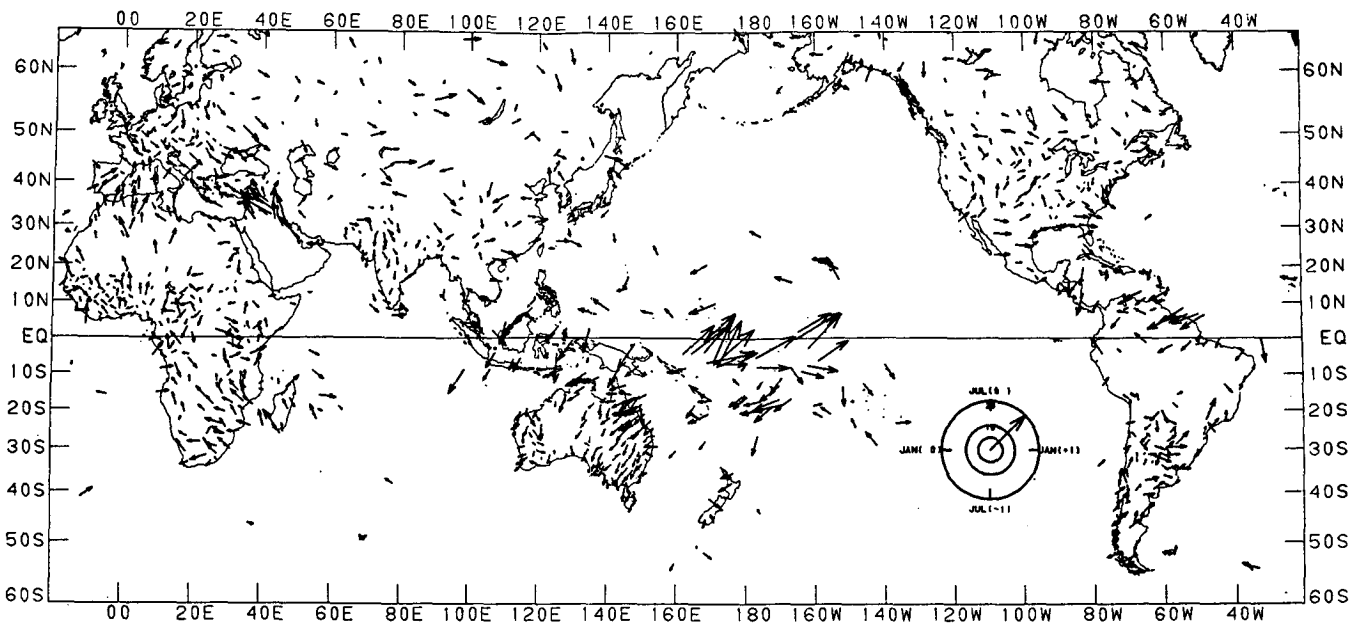

FIG. 1. The amplitudes and phases of ENSO composite ranked precipitation plotted as vectors. The vectors are based on a 24-month harmonic fitted to ranked precipitation composites for ENSO episodes. The phases and relative magnitudes of these vectors are indicated by the "vector clock" in the figure.

with broad areas of the globe that exhibit ENSO-related precipitation anomalies over periods of many months. Small geographical areas or isolated stations with apparent ENSO-precipitation relationships are not considered in the analysis that follows. Areas with strong apparent precipitation relationships over a short time span, i.e., 2 or 3 months, are also not considered for further analysis.

The global nature of the ENSO-related precipitation is revealed by the many regions in which neighboring harmonic vectors have large magnitudes and similar phases (Fig. 1). In high data density areas, only the vector based on the longest data record is plotted in each 2° latitude by 2° longitude subarea. ENSO-related precipitation is especially well indicated in several tropical regions, including Indonesia, the central Pacific, northeastern South America, and eastern Africa. In these regions, the vectors reflect large-scale spatial shifts in tropical convection patterns associated with ENSO. In particular, the ENSO-related eastward shift (Quiroz, 1983b; Barnett, 1984) of precipitation from the western Pacific and Indonesia to the central equatorial Pacific is clearly reflected in the magnitudes and phases of the harmonic vectors over this part of the globe. Vectors in the central Pacific indicate greatly enhanced precipitation, with a maximum in the Northern Hemisphere summer and fall, while extreme dry conditions are indicated over much of Indonesia for the same relative phase of the composite ENSO cycle. [As noted above, the harmonic vectors are formally constrained to point towards the positive (wet) side of the fitted composite, although their practical importance may be on the negative (dry) side of the composite episode as is the case over Indonesia. In these cases, the important ENSO relationship is 180°, or 1 composite year, out of phase with the indicated direction.]

In the subtropics and higher latitudes, there are suggestions of ENSO-related precipitation in India, Australia, parts of Mexico and the United States (Ropelewski and Halpert, 1986), Central America, and Africa. In these areas of the world, the precipitation is likely linked to ENSO and tropical circulation features through indirect processes.

The harmonic vector map, Fig. 1, indicates that large portions of the globe may have ENSO-related behavior. The harmonic vectors are useful to identify areas of the world that may have ENSO-related precipitation but the vector maps are not sufficient, in themselves, to establish the consistency of these relationships. These apparent ENSO-related signals are examined in detail for various regions of the world in the next section.

4. Regional precipitation relationships

Regions of the globe are selected for further analysis on a subjective basis. The selected regions are those for which the precipitation analysis shows relatively large harmonic vector amplitudes with coherent, or similar, phases. The ratio of the mean vector magnitude to the mean scalar magnitude of all the harmonic vectors in an area, i.e., the ratio of the average harmonic vector for the region to the average of the individual vector magnitudes, is taken as a measure of the "coherence" in the selected areas. This "coherence" is analogous to the "directional steadiness" of the wind often used in

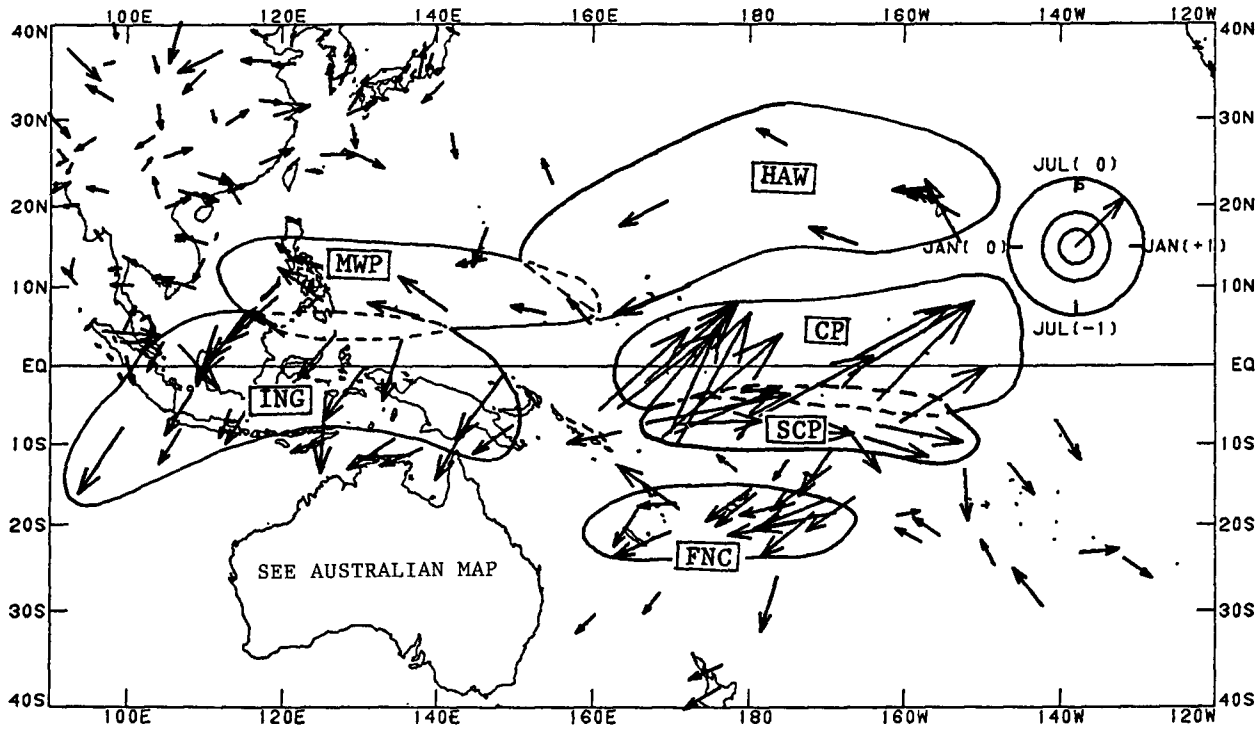

FIG. 2. Subjectively determined "core regions" of consistent ENSO-related precipitation for the Pacific Basin: central Pacific (CP), south central Pacific (SCP), Indonesia–New Guinea (ING), Fiji–New Caledonia (FNC), Micronesia–West Pacific (MWP), and Hawaiian (HAW). Areas of possible overlapping influence or where the boundaries are not well defined are indicated by dashed lines.

tropical analysis, e.g., Hastenrath and Lamb (1977). In North America, consistent ENSO-precipitation relationships were found only in regions for which the "coherence" equaled or exceeded 0.80 (Ropelewski and Halpert, 1986). Thus, in this study, only those areas of relatively high coherence are subjected to the following further analyses:

(i) For each station within a candidate region, time series are formed of monthly precipitation percentiles based on gamma distributions (Ropelewski et al., 1985) fit to the entire data record.

(ii) ENSO composites, formed from each station in the region, are then averaged to form an ENSO "aggregate" composite and plotted. This aggregate composite is used to identify subjectively the "season" within the ENSO cycle with the largest apparent signal and the sign of that signal.

(iii) Time series of station-averaged precipitation percentiles, for the season identified in the previous analysis step, are plotted and examined to determine the consistency of the ENSO-related signal within the region.

Precipitation is expressed as percentiles of a gamma distribution in this part of the analysis because the gamma percentiles represent quantities that are easier to interpret and relate to physical processes while maintaining some of the more desirable features of the percentile ranks. For example, like the percentile ranks, this method of expressing the precipitation effectively removes the annual cycle from the time series.

a. Pacific Basin

A careful examination of the harmonic vector map in the Pacific Basin suggests six regions with homogeneous ENSO-related precipitation (Fig. 2). No regions are identified in the eastern Pacific, at least partly due to the poor data coverage in this area. Dashed lines in Fig. 2 indicate areas of possible overlapping influence and regions where there are not enough station data to define the boundaries. In some of these cases the same station data may be included in the analysis for two regions. The composite ENSO cycle precipitation percentiles for these six core regions (Fig. 3) indicate that in two of them, the central Pacific (CP) and the south central Pacific (SCP), ENSO is associated with increased precipitation. In each of the remaining four regions, Indonesia–New Guinea (ING), Fiji–New Caledonia (FNC), Micronesia–West Pacific (MWP), and Hawaiian (HAW), the ENSO composite suggests decreased precipitation throughout much of the cycle. The harmonic vectors and the ENSO composites in Figs. 3a and 3b suggest some differences in phase between the precipitation in the CP and SCP regions. The composite for the CP suggests that ENSO-related

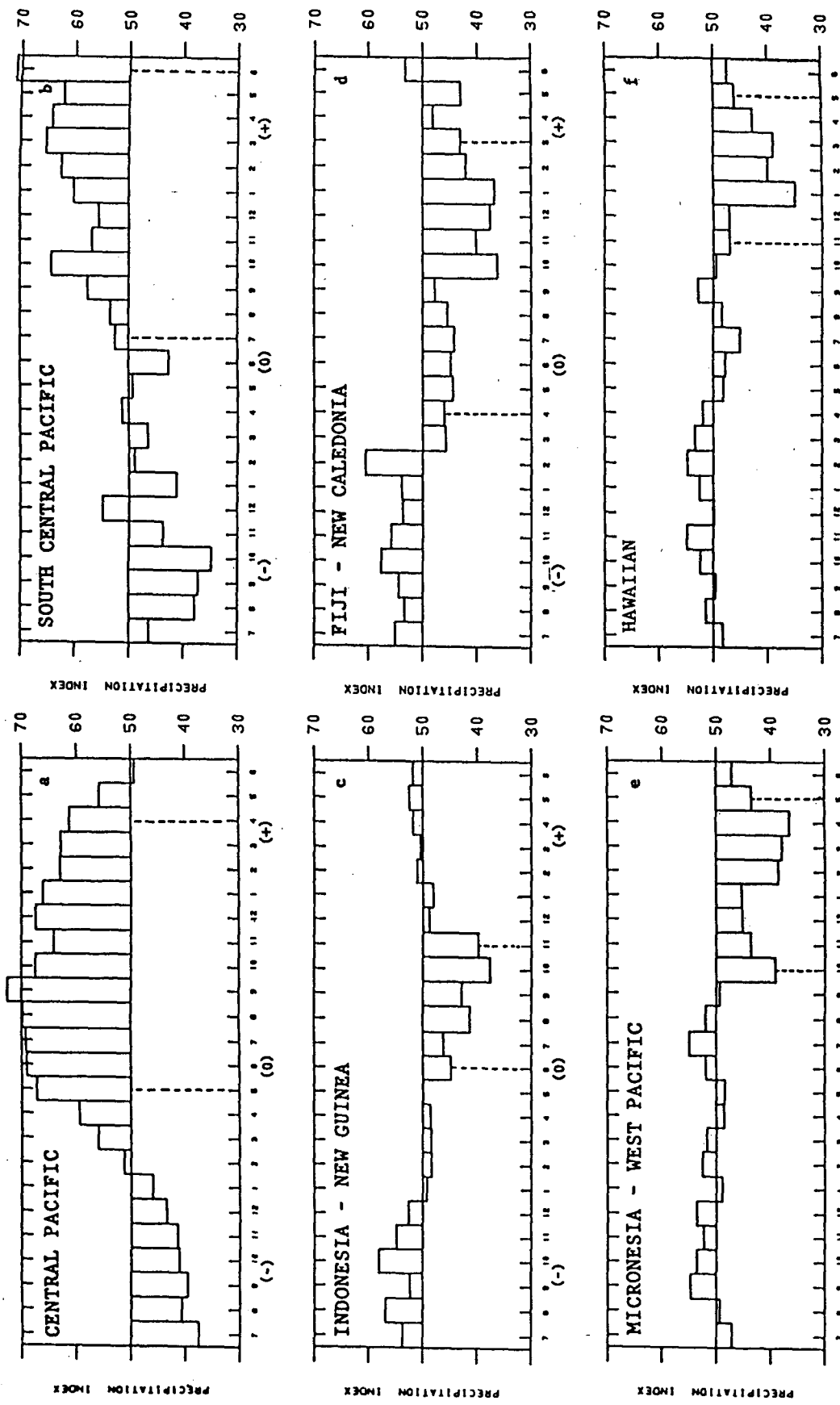

FIG. 3. Composite precipitation index (average gamma percentile) for an idealized 24-month ENSO cycle. Dashed vertical lines indicate the extent of the "season" of most significant ENSO-related precipitation: (a) central Pacific, (b) south central Pacific, (c) Indonesia–New Guinea, (d) Fiji–New Caledonia, (e) Micronesia–West Pacific and (f) Hawaiian.

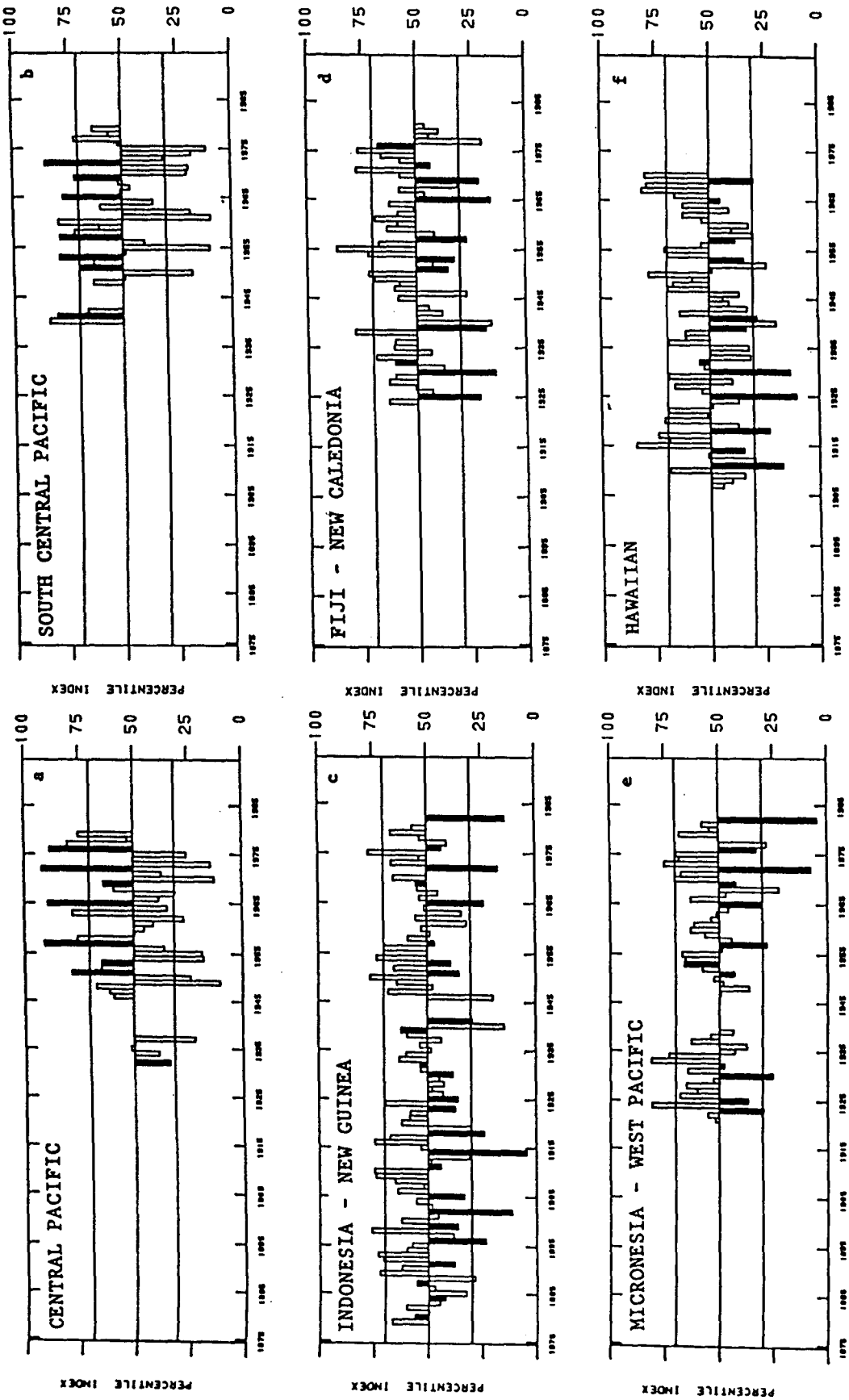

FIG. 4. Precipitation index (average gamma percentile) time series for the Pacific Basin regions: (a) central Pacific—May(0) to Apr(+) season, (b) south central Pacific—Jul(0) to Jun(+), (c) Indonesia–New Guinea—Jun(0) to Nov(0), (d) Fiji–New Caledonia—Apr(0) to Mar(+), (e) Micronesia–West Pacific—Oct(0) to May(+), and (f) Hawaiian—Nov(0) to May(+). The shaded bars represent ENSO years. Results are summarized in Table 2.

precipitation appears as early as February of the ENSO year, Feb(0), in this region. This precipitation may be associated with the eastward progression of convective activity discussed earlier. Such a progression was observed in the 1982/83 episode (Quiroz, 1983b) and is consistent with the early appearance, Jan(0), of drier than normal conditions in the ING composite (Fig. 3c). Enhanced precipitation in the SCP composite does not appear until Jul(0). It is likely that this precipitation enhancement is related to a northward displacement, suggested in the Rasmusson and Carpenter (1982) wind composites, of the South Pacific convergence zone (SPCZ) later in the ENSO cycle. The long period of below normal precipitation in the FNC area ENSO composite (Fig. 3d) is also likely related to the northward displacement of the SPCZ. Some of the individual harmonic vectors suggest that the precipitation deficiency may extend as far south as New Zealand. Gordon (1986), however, finds that the typical ENSO-related precipitation patterns are difficult to define in New Zealand owing to complex orographic and other local and seasonal influences. Thus, New Zealand is left out of the core areas. Drier than normal conditions related to ENSO are also indicated for the two Pacific regions which are located north of the equator, the MWP and HAW. Composites for both of these regions, Figs. 3e and 3f, indicate that the Oct(0) to May(+) ENSO season tends to be dry. There are not enough station data in this part of the Pacific to ascertain whether the MWP and HAW regions are parts of the same continuous region or are two separate areas, both related to ENSO during the same phase of the composite cycle.

Time series for each of these Pacific basin regions for the "seasons" identified in the composites indicate the high degree of consistent ENSO-related precipitation departures (Fig. 4). Different numbers of stations are available to form averages and composites for each region. Because a minimum of five stations is required to represent a region, the length of the time series depicted in each of Figs. 4a–f varies from region to region. The time series for the CP and SCP regions confirm the tendency for enhanced ENSO-related precipitation, while the time series of ING and the remaining three Pacific regions each show highly consistent occurrences of negative precipitation departures related to ENSO.

TABLE 2. Summary of ENSO-related precipitation for selected regions of the globe.

Region		Season	Coherence	Number of episodes		
				Total	Wet	Dry
		Pacific Basin				
Central Pacific	(CP)	May(0)–Apr(+)	0.98	8	7	1
South Central Pacific	(SCP)	Jul(0)–Jun(+)	0.88	8	8	0
Indonesia–New Guinea	(ING)	Jun(0)–Nov(0)	0.82	25	5	20
Fiji–New Caledonia	(FNC)	Oct(0)–Mar(+)	0.95	11	2	9
Micronesia–W. Pacific	(MWP)	Oct(0)–May(+)	0.91	13	1	12
Hawaiian	(HAW)	Nov(0)–May(+)	0.88	11	2	9
		Australia				
Northern Australia	(NAU)	Sep(0)–Mar(+)	0.95	26	4	22
Eastern Australia	(EAU)	Sep(0)–Feb(+)	0.89	26	6	20
S Australia–Tasmania	(SAT)	May(0)–Oct(0)	0.94	24	6	18
Central Australia	(CAU)	Mar(0)–Feb(+)	0.86	26	7	19
		Indian Subcontinent				
India	(IND)	Jun(0)–Sep(0)	0.86	26	5	21
Minicoy–Sri Lanka	(MSL)	Oct(0)–Dec(0)	0.92	26	21	5
		Tropical and southern Africa				
East Equatorial Africa	(EEQ)	Oct(0)–Apr(+)	0.93	13	11	2
Southeast Africa	(SEA)	Nov(0)–May(+)	0.90	22	5	17
		South America				
Northeastern SA	(NSA)	Jul(0)–Mar(+)	0.91	17	1	16
Southeastern SA	(SSA)	Nov(0)–Feb(+)	0.82	19	18	1
		Central America				
Central America–Caribbean	(CEN)	Jul(0)–Oct(0)	0.77	19	5	14
		North America*				
Great Basin		Apr(0)–Oct(0)	0.80	11	9	2
Gulf and N Mexico		Oct(0)–Mar(+)	0.93	22	18	4

* From Ropelewski and Halpert, 1986.

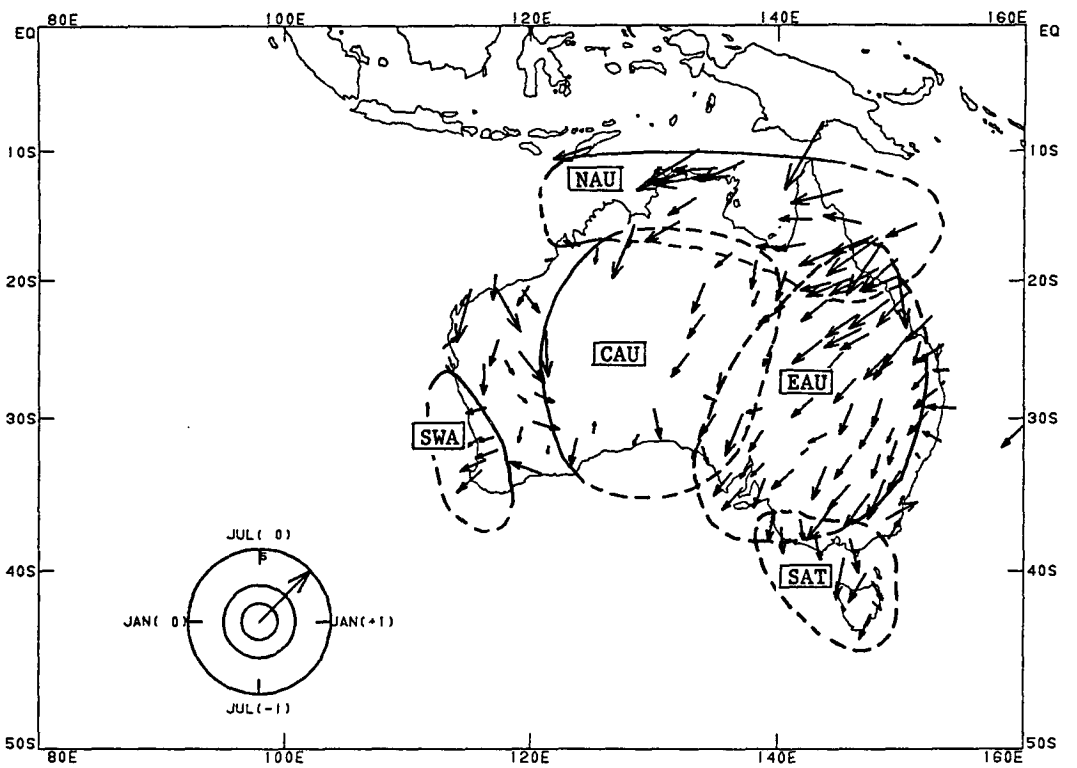

FIG. 5. As in Fig. 2 except for the "core regions" in Australia: northern Australia (NAU), eastern Australia (EAU), southern Australia–Tasmania (SAT), central Australia (CAU), and (e) southwestern Australia (SWA).

A summary of these time series (Table 2) shows that the precipitation departures are in the direction indicated by the ENSO composites for at least 80% of the ENSO episodes for each of the core areas. We note that 1932 is the only ENSO year to show an atypical precipitation anomaly in each of the Pacific Basin regions. This casts some doubt as to whether the 1932 ENSO was a typical episode.

b. Australia

The large number of precipitation stations with long periods of record (over 200 stations, 51 of which have time series covering 25 ENSOs) provides the basis for defining five core regions over Australia (Fig. 5). Most of the harmonic vectors depicted in Fig. 5 are based on data covering at least 18 ENSO events for time series starting before 1900. The boundaries of the core regions are subjectively determined on the basis of phase differences in the ENSO harmonic vectors. Overlapping boundaries between regions indicate that these boundaries are not well defined. The areas defined by the harmonic vectors are, in general, consistent with those defined in the ENSO–Australian correlation studies of McBride and Nicholls (1983). As in that study, we find that the ENSO-related precipitation signal is not well defined for areas east of the Great Dividing Range.

ENSO composites for the Australian regions (Fig. 6) indicate that dry conditions tend to be associated with ENSO over most of the continent. The composites for northern Australia (NAU), eastern Australia (EAU), and central Australia (CAU) suggest that dry conditions may begin fairly early in the ENSO composite cycle, i.e., Jan(0) to Feb(0), but that the strongest consistent anomalies do not assert themselves until Sep(0). The indication of a dry ENSO-related precipitation anomaly in NAU through the southern winter, Jun(0) to Aug(0), is not very significant in terms of absolute precipitation amounts since winter is normally a very dry season in this part of Australia. Precipitation is more uniformly distributed throughout the year in most parts of EAU so that the indications of a dry ENSO composite continuing through the southern winter may be more meaningful. The ENSO composite for the mid-latitude southern Australia–Tasmania (SAT) region suggests a much shorter period of ENSO-related precipitation than those discussed above. The ENSO composite for southwestern Australia (SWA) does not show as clearly defined an ENSO-related precipitation season as the other areas under consideration, i.e., the tendency for drier than normal conditions for the Jul(0) to Sep(0) season is not significantly different than a similar dry period later in the composite. Thus, SWA is excluded from further analysis in this study.

The precipitation percentile time series for NAU for the Sep(0) to Mar(+) season (Fig. 7a) confirms that the overwhelming majority of ENSO episodes, 22 out of 26, are associated with dry conditions in this region.

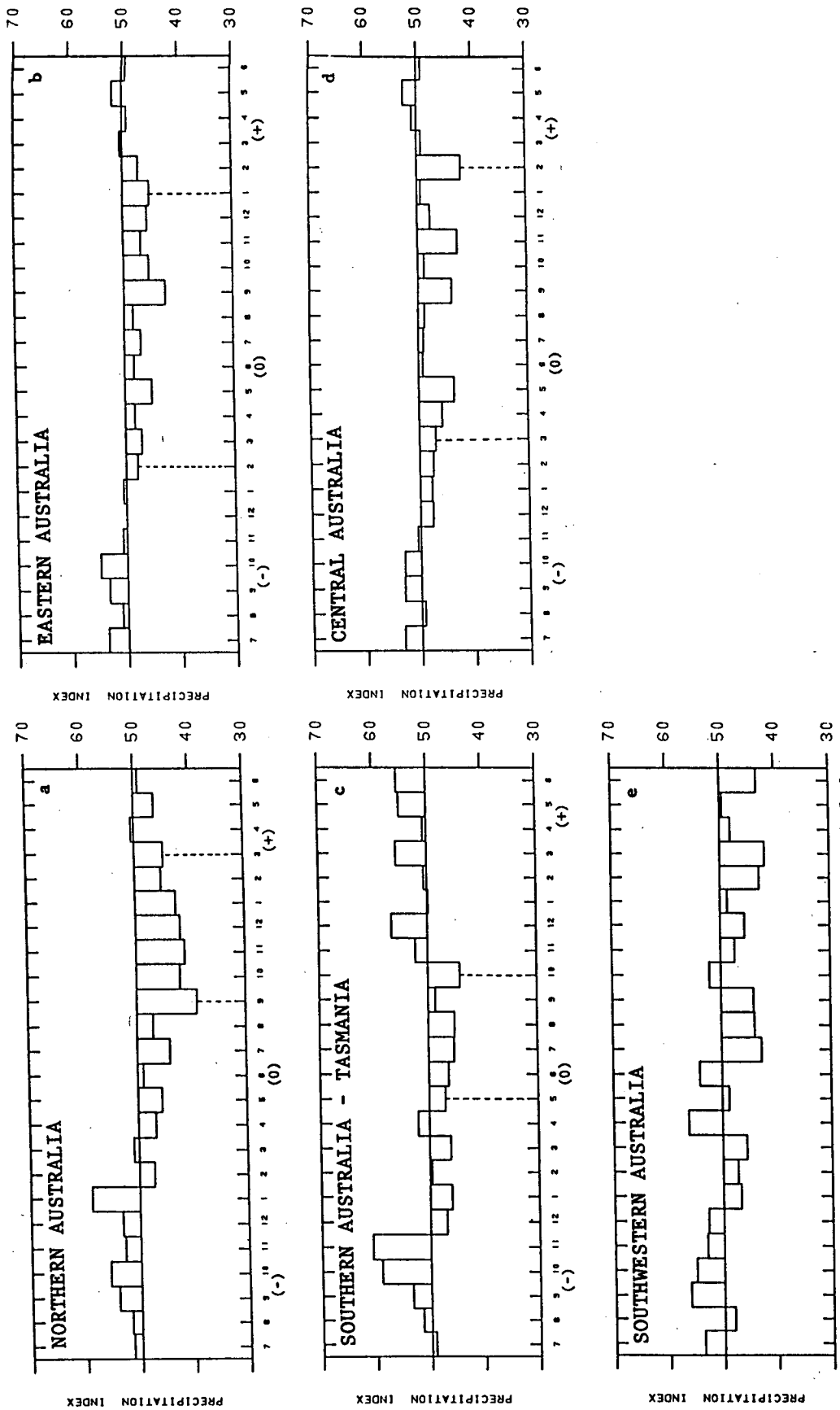

FIG. 6. As in Fig. 3 except for Australian regions: (a) NAU, (b) EAU, (c) SAT, (d) CAU and (e) SWA.

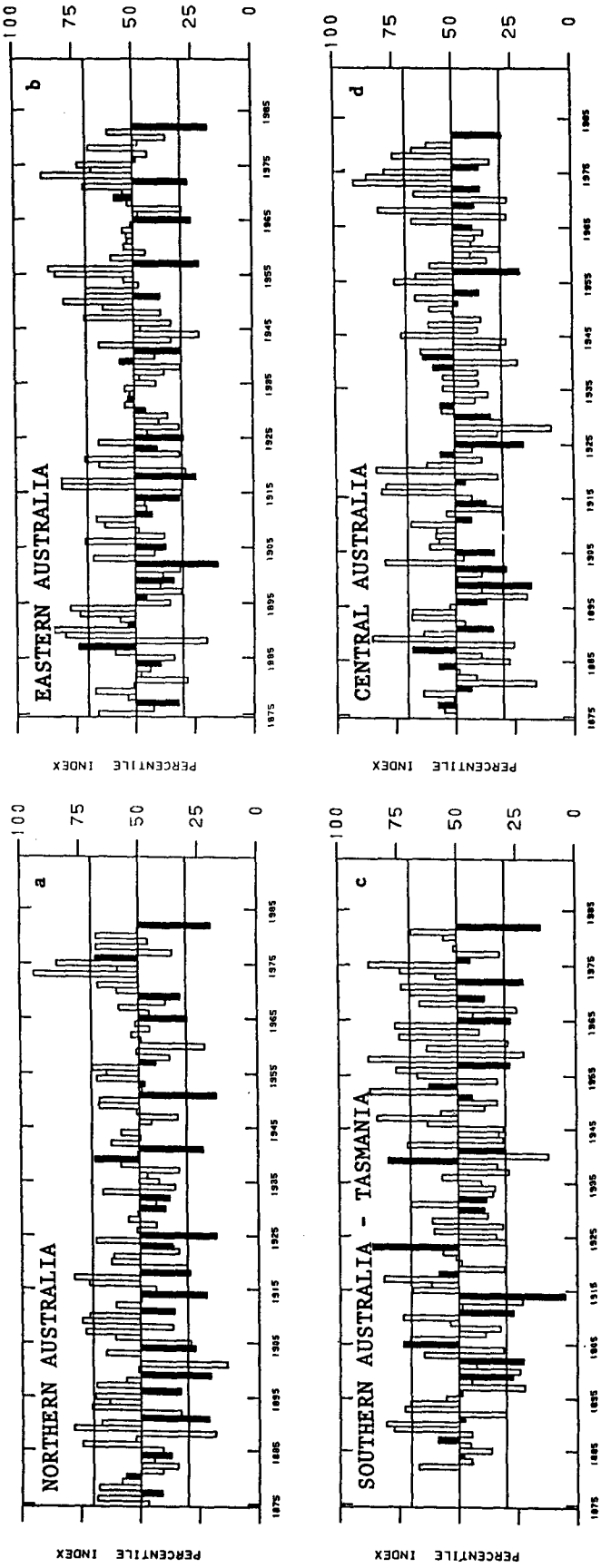

FIG. 7. As in Fig. 4 except these are precipitation time series for the Australian regions: (a) northern Australia—Sep(0) to Mar(+), (b) eastern Australia—Feb(0) to Jan(+), (c) southern Australia–Tasmania—May(0) to Oct(0) and (d) central Australia—Mar(0) to Feb(+).

The time series for the longer Apr(0) to Mar(+) season (not shown) is almost identical to the shorter season series, confirming that the significant ENSO-related precipitation anomaly is associated with the disruption of the northern Australian spring and summer monsoon. The precipitation time series for EAU for Feb(0) to Jan(+) (Fig. 7b) also shows a consistent ENSO relationship—20 dry seasons out of 26 episodes. The ENSO-related precipitation in EAU is remarkable not only for the length of the "season" which shows an ENSO-related anomaly, but also because this region spans an area from the subtropics through the midlatitudes. The time series for the mid-latitude SAT region (Fig. 7c) shows 18 dry May(0) to Oct(0) seasons out of 24 (Table 2). The appearance of large positive precipitation index values associated with three of the episodes is an indication that factors other than ENSO may influence the precipitation at higher latitudes and that the typical ENSO-related patterns may be more highly variable at these latitudes. Nevertheless, half of the 16 driest May(0) to Oct(0) seasons are ENSO years, attesting to the strong influence of this phenomenon over the region. It is somewhat surprising that the time series for CAU (Fig. 7d), which includes both the Simpson and Great Western Deserts, also shows a very consistent ENSO-related precipitation relationship. While precipitation in CAU is more uniformly distributed throughout the year than in NAU, average amounts are generally quite small. The fact that the ENSO relationships are apparent in the CAU and EAU time series may in part be related to the fact that the "seasons" span 12 months. Thus, phase differences of a few months in the evolution of the individual episodes are not apt to change the character of this "seasonal" ENSO-related precipitation.

c. *Indian subcontinent*

The harmonic vectors suggest an ENSO-related summer monsoon precipitation deficiency in northern, central, and peninsular India (IND) and enhanced ENSO-related winter monsoon precipitation in extreme southern India, Sri Lanka, and Minicoy (MSL), Fig. 8. The areas of implied ENSO-related precipitation anomalies revealed by this analysis are consistent with those of several studies relating the Southern Oscillation to monsoon precipitation over India, including the recent studies of Rasmusson and Carpenter (1983) and Shukla and Paolino (1983). The precipitation station network used in this study does not provide as accurate an estimate of the magnitude of precipitation anomalies over India as the area-averaged precipitation data of Rasmusson–Carpenter and Shukla–Paolino, and thus the ENSO composites and precipitation time series are

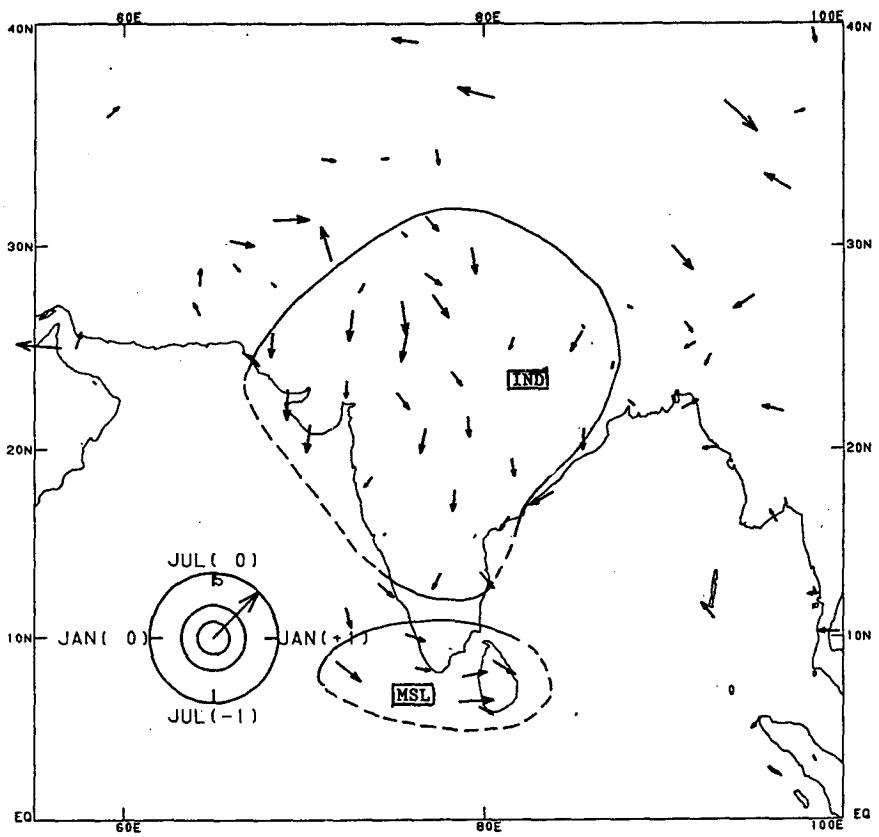

FIG. 8. As in Fig. 2 except for the Indian subcontinent.

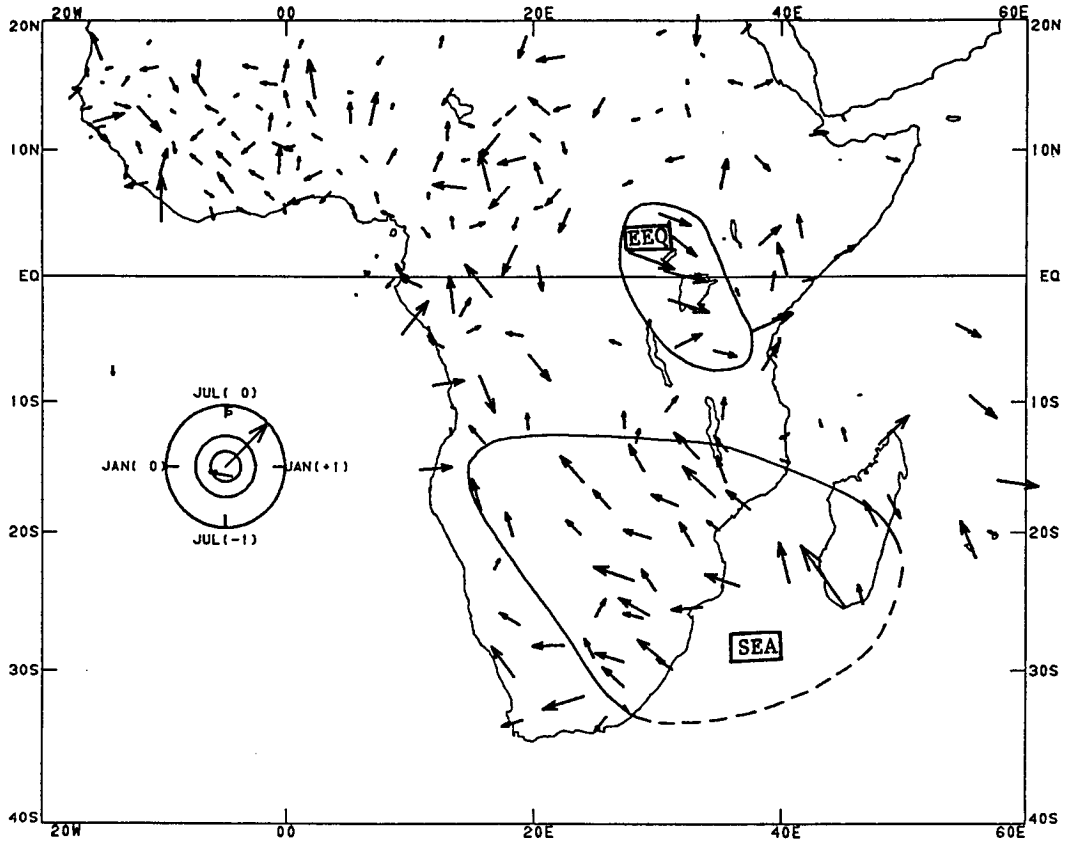

FIG. 9. As in Fig. 2 except for equatorial and southern Africa.

not presented here. Nevertheless, as noted in Table 2, the ENSO-related precipitation record based on the station network is consistent with these other two studies. Dry northern summer monsoons were experienced in the IND core region during 21 out of 26 ENSO episodes (versus 19 dry out of 25 in Rasmusson and Carpenter), and wet fall and early winter rains are associated with 21 out of 26 ENSOs in the MSL region.

d. Tropical and southern Africa

The map of harmonic analysis vectors for this region (Fig. 9) suggests two areas of ENSO-related precipitation over tropical and southern Africa. The equatorial eastern African (EEQ) region encompasses parts of Kenya, Uganda, Rwanda, Burundi and Tanzania, while the southeastern Africa (SEA) region includes portions of all African nations south of 15°S. This analysis does not suggest any large coherent areas of ENSO-related precipitation in the Sahel region. Interannual variations in Sahelian rainfall have been linked to Atlantic Ocean sea surface temperature anomaly patterns (e.g., Lough, 1986), and thus ENSO-precipitation relationships, if they exist, would be difficult to separate from the Atlantic SST relationships. ENSO-related precipitation in the Sahel would also be difficult to uncover in this analysis because of the long-term negative trend in precipitation (Nicholson, 1985; Lamb, 1982), which would serve to confound any ENSO precipitation relationships.

The ENSO composite precipitation percentiles for EEQ (Fig. 10a) indicate that this region tends to experience greater than normal precipitation in the Oct(0) to Apr(+) period of the idealized ENSO cycle. An examination of the monthly mean precipitation for stations within the EEQ region indicates that many locations in this region have 2 rainy seasons, corresponding roughly to the sun's equator crossing times. Thus, the Oct(0) to Apr(+) "season" includes parts of both rainy seasons. The time series of mean precipitation percentiles for this region (Fig. 11a) shows 11 out of 13 seasons are associated with above normal precipitation. If the "season" is split into subseasons, Oct(0) to Dec(0) and Jan(+) to Apr(+), the earlier subseason shows a stronger ENSO relationship, 10 above normal out of 14, than the later subseason, 7 above normal out of 13.

The ENSO composite precipitation percentiles for the SEA region (Fig. 10b) indicate that drier than normal conditions are associated with ENSO for the Nov(0) to May(+) "season." Thus, SEA tends to experience dry conditions during roughly the same "sea-

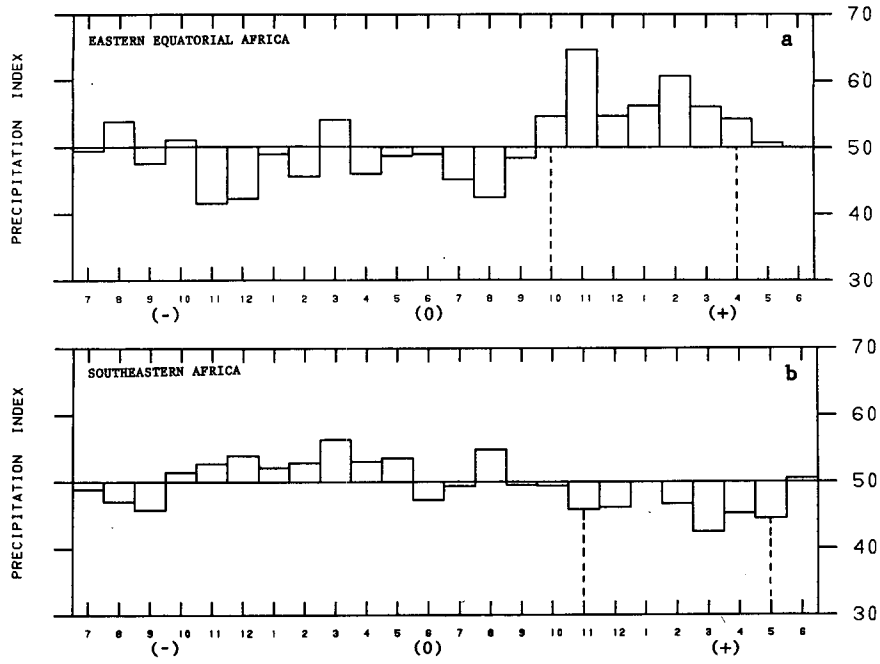

FIG. 10. As in Fig. 3 except for the African regions: (a) eastern equatorial Africa and (b) southeastern Africa.

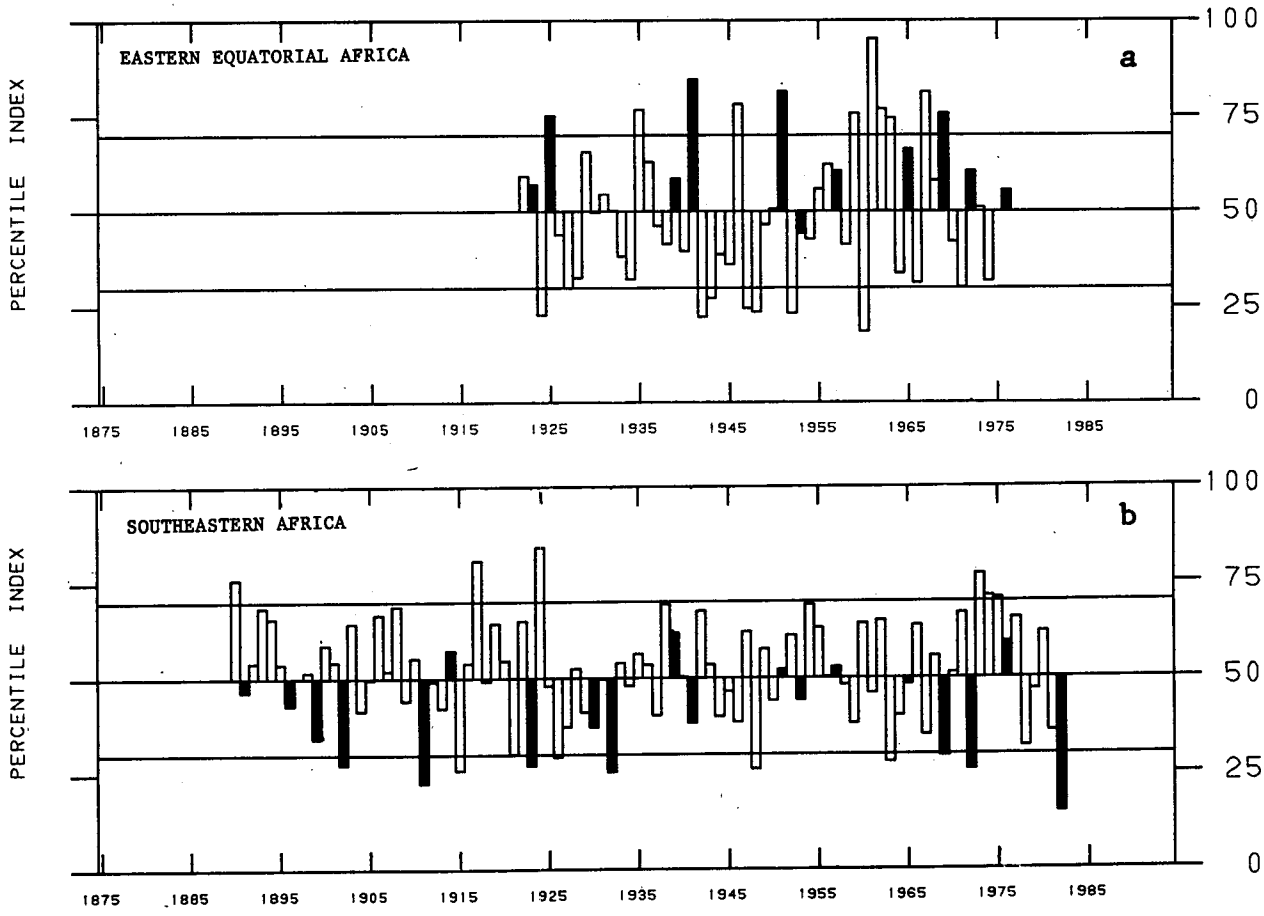

FIG. 11. As in Fig. 4 except that the precipitation time series are for the African core regions: (a) eastern equatorial Africa—Oct(0) to Apr(+) and (b) southeastern Africa—Nov(0) to May(+).

son" that EEQ experiences wetter than normal conditions. ENSO composite divergence patterns in the Pacific (Rasmusson and Carpenter, 1982) indicate that ENSO is associated wiith an equatorward shift of the intertropical convergence zone (ITCZ) and the SPCZ. Another convergence zone often appears from southern Africa south-southwestward into the Natal basin (Dhonneur, 1974). The wet and dry patterns for the EEQ and SEA regions of Africa are consistent with an equatorward shift of this convergence zone. Precipitation percentile time series for SEA (Fig. 11b) show 17 dry ENSO seasons out of 22. Of the 11 driest Nov(0) to May(+) seasons, 7 occur during ENSO episodes.

There is a suggestion in both of the ENSO cycle composites (Fig. 10) that the ENSO-related African precipitation in these two regions might have some predictive utility. The EEQ composite shows a tendency for dry conditions in the same "season" preceding ENSO episodes; and, conversely, the SEA composite shows wet conditions. An examination of the time series for these regions (Fig. 11a–b), however, clearly demonstrates that these suggested relationships do not hold and are an artifact of the analysis method. (For example, in EEQ only 6 "wet" ENSO episodes are preceded by dry "seasons" and in SEA only 13 "dry" ENSOs are preceded by wet "seasons.")

e. Northern Africa, southern Europe, Mid-East

The map of harmonic vectors for this portion of the globe (Fig. 12) shows two relatively large, coherent regions suggestive of ENSO-related precipitation: northern Africa–southern Europe (NAS) and the Mediterranean Mid-East (MME). The implied ENSO relationships in these regions are difficult to understand or attribute to any of the known ENSO-related atmospheric circulation changes. The ENSO precipitation percentile composite for NAS (Fig. 13a) defines a "season," Apr(0) to Nov(0), which spans the driest months of the year including those that have zero mean precipitation. The corresponding time series for the NAS region (Fig. 14a) indicates that this apparent ENSO relationship has not been stable throughout the historical data record. Previous to 1940, the time series indicates an almost equal number of wet and dry "seasons" associated with ENSO—10 and 7, respectively. The post-1940 record shows a preponderance of wet "seasons" associated with ENSO, i.e., 8 out of 9. The change in character of the time series between the two eras is also reflected in the relation between ENSO and sea level pressure over southern Europe (van Loon and Madden, 1981). The lack of a clear physical mechanism to account for ENSO-related precipitation in the NAS region also suggests that this apparent relationship may result from undocumented errors in the data or simply may be an artifact of the empirical analysis method. In particular, the large number of months with zero precipitation serves to confound the ranking scheme and subsequent determination of a meaningful first harmonic.

The ENSO composite precipitation percentiles for the MME region (Fig. 13b) suggest a very short "season," Apr(0) to Jul(0), with an apparent ENSO-precipitation relationship. This "season" also spans the driest months of the year, including months with zero mean precipitation, at some stations. The time series for this "season" (Fig. 14b) shows unexplained shifts in the character of the implied ENSO-precipitation relationship. In particular, the sign of the ENSO-precipitation anomalies for the 1932–53 period is opposite to that of the implied anomalies for both the earlier and later periods. These secular changes in the direction of the implied ENSO-precipitation relationship in MME limit their usefulness and cast doubt as to whether they reflect physical changes in ENSO-related precipitation.

The subjective analysis of harmonic vectors identifies two regions which, upon closer examination of the data,

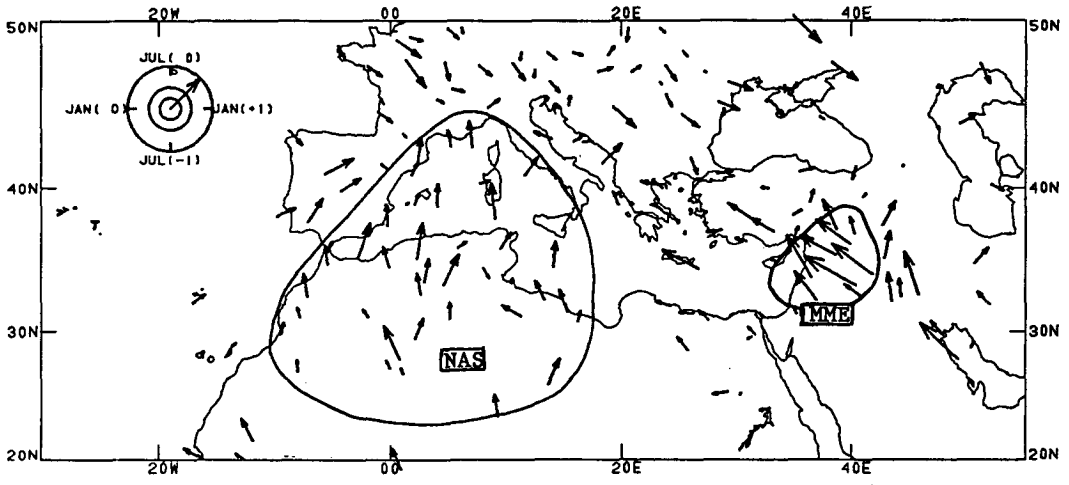

FIG. 12. As in Fig. 2 except for northern Africa–southern Europe, and the Mediterranean Mid-East.

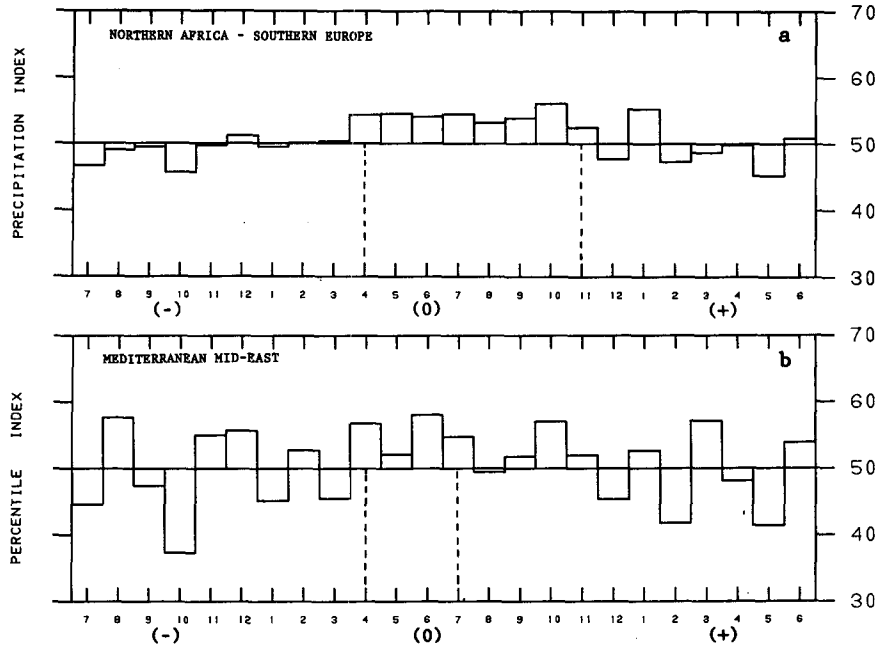

FIG. 13. As in Fig. 3 except for the regions: (a) northern Africa-southern Europe (NAS) and (b) the Mediterranean Mid-East (MME).

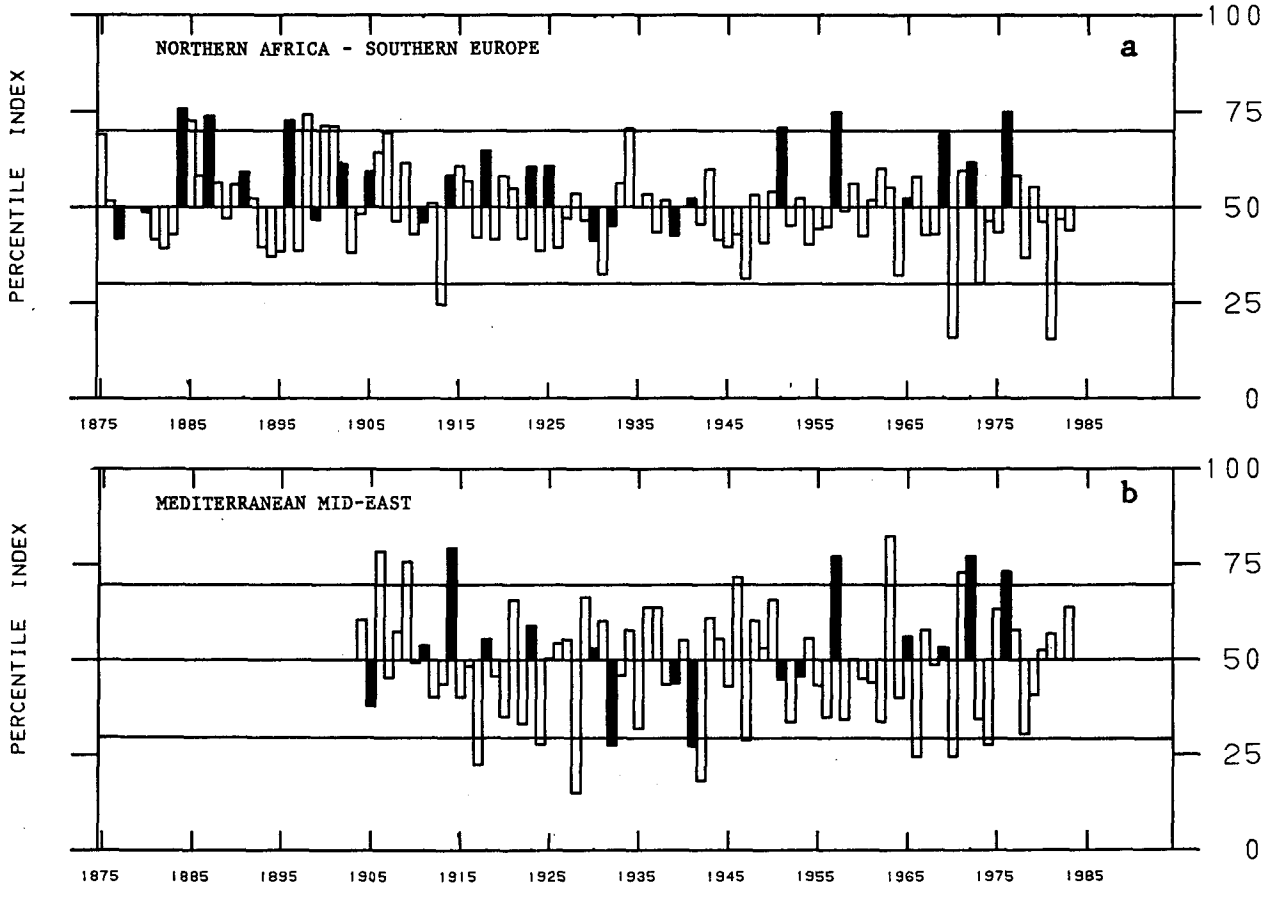

FIG. 14. As in Fig. 4 except that the time series are for the core regions: (a) northern Africa–southern Europe—Apr(0) to Nov(0) and (b) Mediterranean Mid-East—Apr(0) to Jul(0).

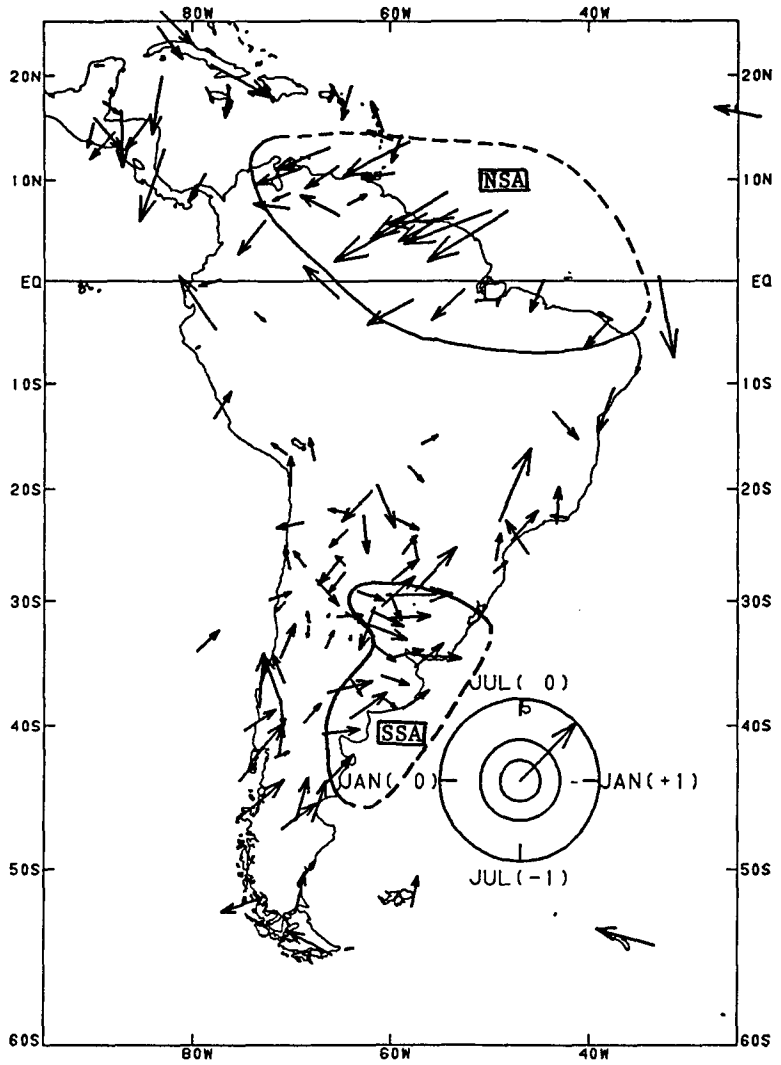

FIG. 15. As in Fig. 2 except for South America.

show ENSO-relationships that are unstable over time. This points out the limitations of identifying regions of ENSO-related precipitation based on the harmonic analysis alone, particularly in desert areas of the world, and underscores the necessity of examining the precipitation time series.

f. South America

The map of harmonic vectors for South America (Fig. 15) indicates two areas of likely ENSO-related precipitation: northeastern South America (NSA) and southeastern South America (SSA). A sufficiently dense network of surface stations was not available in this analysis to define regions for the western coastal countries of Ecuador and Peru which have a well-documented ENSO–precipitation relationship (e.g., Hastenrath, 1978). Data are also insufficient for a detailed analysis of the interior Amazon basin regions of Brazil.

The ENSO precipitation composite for NSA, which includes north equatorial Brazil, French Guiana, Surinam, Guyana, and Venezuela, shows a clearly defined precipitation deficiency for the Jul(0) to Mar(+) "season" (Fig. 16a). The corresponding precipitation time series (Fig. 17a) indicates that this region has one of the most consistent ENSO-precipitation relationships of any discussed in this paper with 16 dry episodes out of 17 ENSOs (Table 2). This result is consistent with Hastenrath and Heller (1977), who found a relationship between drought in Northeast Brazil and ENSO. The strength of the ENSO relationship in NSA is further evidenced by the fact that 9 out of the 11 driest "seasons" occurred in association with ENSO, and none of the wettest "seasons" appear during ENSO years. A study by Kousky et al. (1984) suggests that this lack of precipitation may be due to increased atmospheric subsidence over northern South America associated

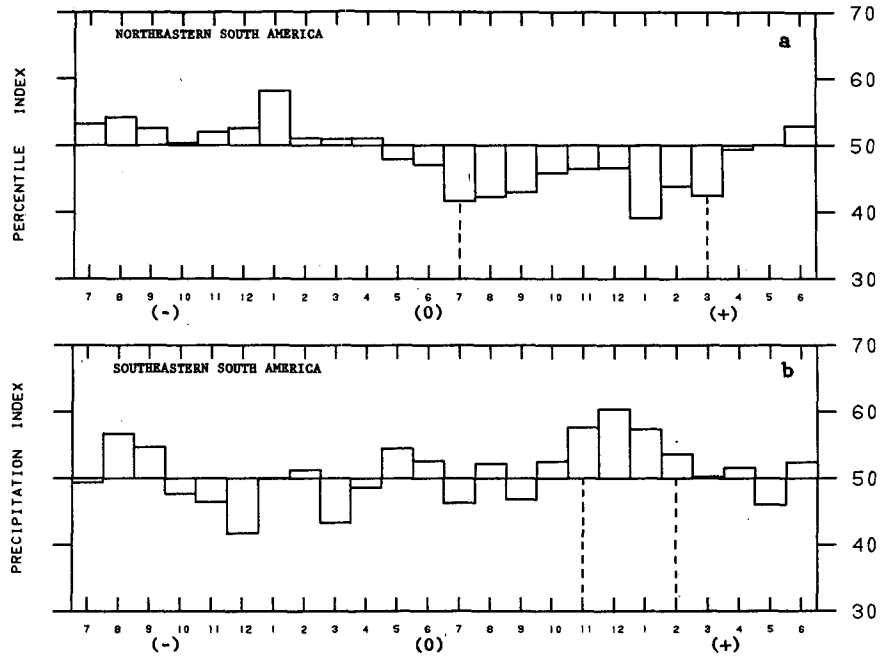

FIG. 16. As in Fig. 3 except for the core regions: (a) northeastern South America (NSA) and (b) southeastern South America (SSA).

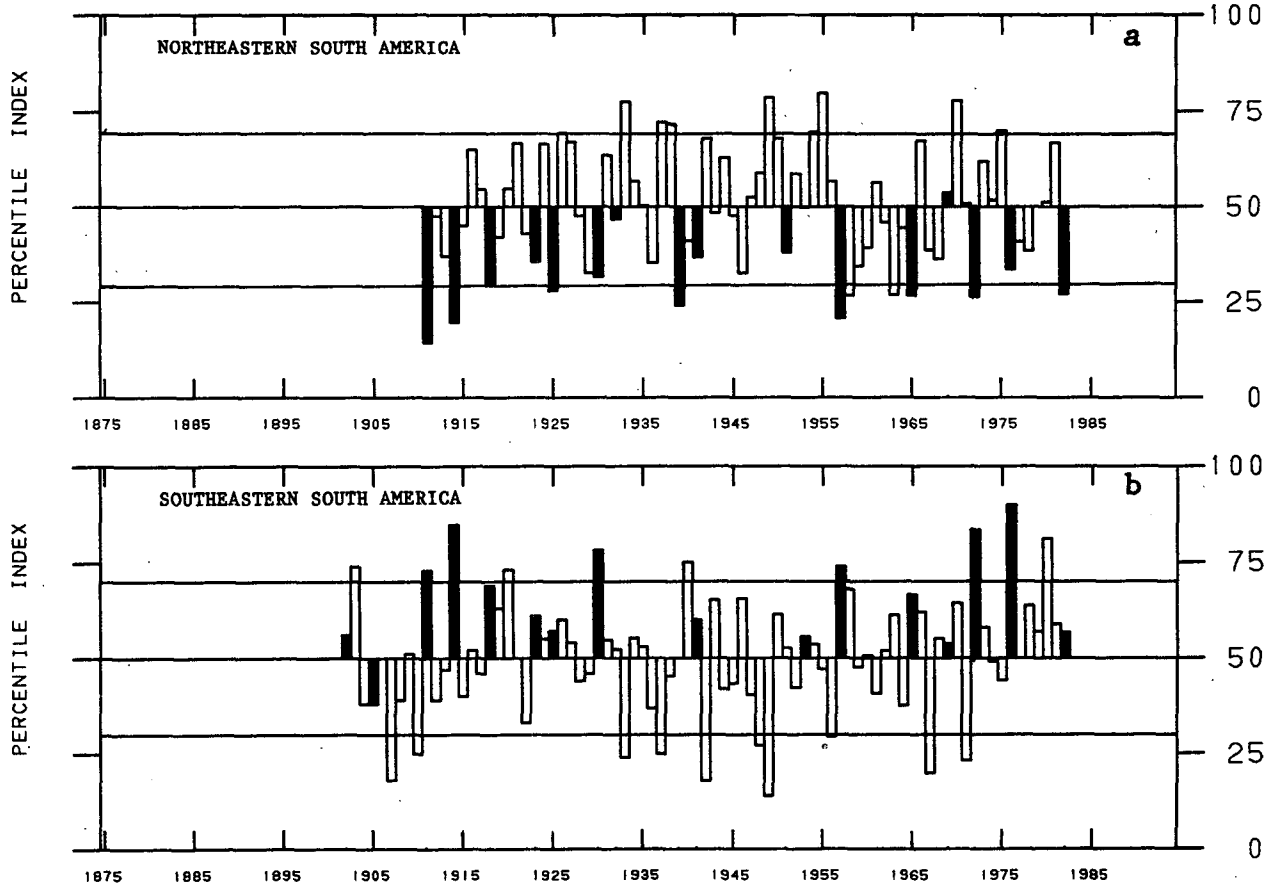

FIG. 17. As in Fig. 4 except that the time series are for the core regions: (a) northeastern South America—Jul(0) to Mar(+) and (b) southeastern South America—Nov(0) to Feb(0).

with a westward displacement of the Atlantic Walker circulation during ENSO episodes.

In the SSA region, which includes southern Brazil, Uruguay, and parts of northeastern Argentina, the harmonic vectors do not indicate as strong a relationship as in NSA. This is reflected by a relatively low coherence for the region of 0.81. The ENSO composite for SSA (Fig. 16b), however, shows a clear tendency for enhanced precipitation during the Nov(0) to Feb(+) "season" and the time series (Fig. 17b) indicates that this ENSO relationship is very consistent—14 wet episodes out of 16 ENSOs. The ENSO-related enhanced precipitation in SSA may be linked to the stronger than normal 200 mb subtropical westerly winds which tend to occur in association with ENSO (Arkin, 1982). The enhanced westerlies may, in turn, be associated with a south–southeastward oriented convergence zone that often occurs with precipitation in the SSA region (Kousky et al., 1984). Enhanced precipitation in SSA during the 1982/83 episode was confined to a fairly narrow band (Quiroz, 1983b). If the narrow precipitation pattern which occurred during the 1982/83 ENSO is typical, then the SSA area of Fig. 15 might be interpreted as the geographical *range* over which precipitation is related to ENSO rather than as an extended area typically experiencing increased precipitation with each ENSO episode. The occurrence of enhanced ENSO-related precipitation over a narrow band might also account for the relatively low coherence for the region.

g. *Central America and Caribbean*

An examination of the harmonic vectors for Central America and the Caribbean (Fig. 18) suggests a region of ENSO-related precipitation extending from southern Mexico and Guatemala southward into Panama and eastward into the Caribbean. This Central America–Caribbean (CEN) core region is in close proximity to areas of demonstrated ENSO-related precipitation both to the north (Ropelewski and Halpert, 1986) and south (the NSA region discussed above). The CEN region shows the lowest coherence, 0.77, of any discussed in this paper and, were it not for its close proximity to other regions of consistent ENSO-related precipitation, it would not have been considered. The ENSO composite precipitation percentiles (Fig. 19) imply a dry ENSO signal for the Jul(0) to Oct(0) "season," which is in phase with the early part of the dry ENSO signal in NSA. The corresponding time series (Fig. 20) may be interpreted as a tendency for drier than normal conditions: 14 dry "seasons" out of 19, with 5 out of the 9 driest "seasons" being years associated with ENSO.

5. Summary and conclusions

The first harmonic fitted to station precipitation data, expressed as percentile ranks, over an idealized 2-year composite ENSO cycle is used to identify 17 global core regions that appear to have a clear ENSO-precipitation relationship. Two other regions which show an ENSO precipitation relationship, the Gulf and Mexican and the Great Basin of the United States, were discussed in an earlier paper (Ropelewski and Halpert, 1986). The harmonic analysis is not sufficient, in itself, to establish the consistency of an implied ENSO-precipitation relationship and thus further analyses are required. ENSO composites of precipitation in the core regions are used to identify the appropriate season of the relationship suggested by the harmonic vectors. Time series are then plotted to examine the consistency of these ENSO-precipitation signals. These results are summarized in Table 2 and presented in schematic form in Fig. 21. In Fig. 21, areas with similar ENSO-precipitation relationships are combined even though the detailed regional analyses show some differences in the phase of these relationships. As to be expected, the most extensive areas with such relationships are located in the western and central equatorial Pacific, including most of the Australian subtropics. Other areas of the tropics with consistent ENSO-related precipitation variations include northern South America, eastern equatorial Africa, and southern India, Sri Lanka, and neighboring islands. Precipitation relationships at higher latitudes are found in the southeastern sections of each of the Southern Hemisphere land masses: southern Africa, Australia, and South America.

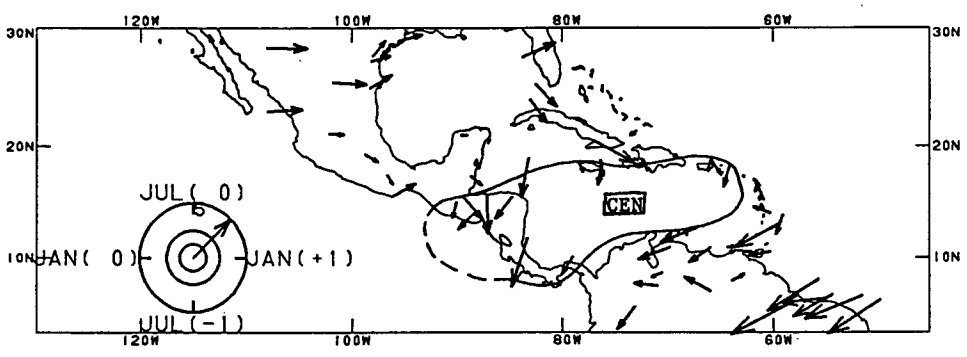

FIG. 18. As in Fig. 2 except for Central America and the Caribbean.

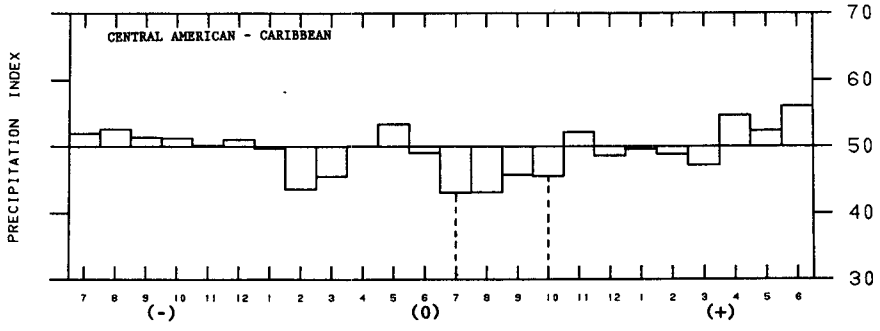

FIG. 19. As in Fig. 3 except for the Central American–Caribbean (CEN) region.

It is clear from these results that global variations in the tropical rainfall patterns are related to ENSO. Mid-latitude precipitation and ENSO are linked for all the major land masses of the Southern Hemisphere but are only evident over the Indian subcontinent and parts of North America in the Northern Hemisphere. The consistency and magnitude of the precipitation relationships suggest that the results of this study have practical utility for forecasting precipitation over the core areas once it has been established that an ENSO episode is in progress. The key to the success of the empirical methods described in this paper is that the "core" regions and "seasons" of ENSO-related precipitation are themselves determined by the analysis. The results discussed here hold for the broad areas and seasons described in the body of the paper, but precipitation time series from individual stations can show substantial variations from episode to episode. It is difficult to establish the statistical significance of the ENSO–precipitation relationships discussed in this paper in any meaningful way. While each of the relationships summarized in Table 2 are no doubt highly significant in terms of standard statistical tests, such tests are not appropriate to the a posteriori results presented here.

Precipitation data for the 1982/83 ENSO episode were not included in the composites on which the harmonic vectors are based, but most of the areas with indications of strong precipitation–ENSO relationships in this analysis are also those which were influenced by the 1982/83 episode (Quiroz, 1983b; Chen, 1983; Ropelewski, 1984; Bergman, 1984). Another independent indication that the analysis identifies areas with ENSO-related precipitation can be found in the outgoing longwave radiation (OLR) studies of Lau and Chan (1983). Anomalies in OLR are related to variations in convective precipitation in the tropics. Although based on a relatively short period of record (6 years), the Lau and Chan study found large variations in OLR in the central Pacific over those areas identified as having increased ENSO-related precipitation in this study. Maps of the correlations between OLR in the central Pacific and OLR over regions of the globe show patterns similar to those discussed here.

Finally, a brief summary of two additional limitations of this type of analysis is appropriate. The analysis method described here does not identify regions of the globe over which the magnitude of ENSO-related precipitation anomalies may be large but vary in sign from episode to episode. The western United States may be an example of such a region, i.e., extremely dry conditions occurred with the 1976 episode, while anomalous wet conditions occurred in conjunction with the 1982 episode (Ropelewski, 1986). Another limitation is that the analysis is very much at the mercy of available station data. Thus, we were not able to identify all the regions of the globe that may have consistent ENSO-related precipitation but for which little or no

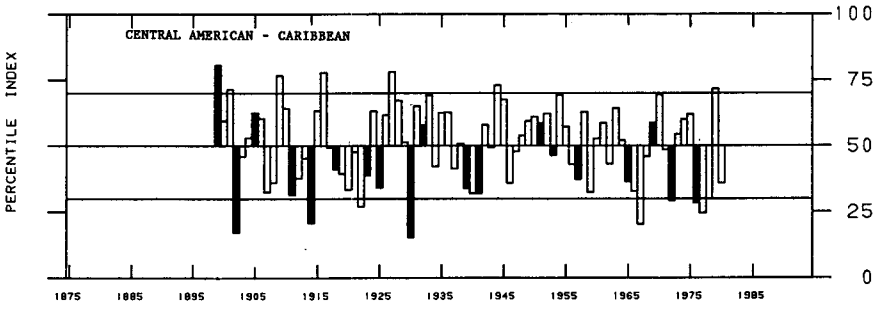

FIG. 20. As in Fig. 4 except that the time series is for the CEN region—Jul(0) to Oct(0).

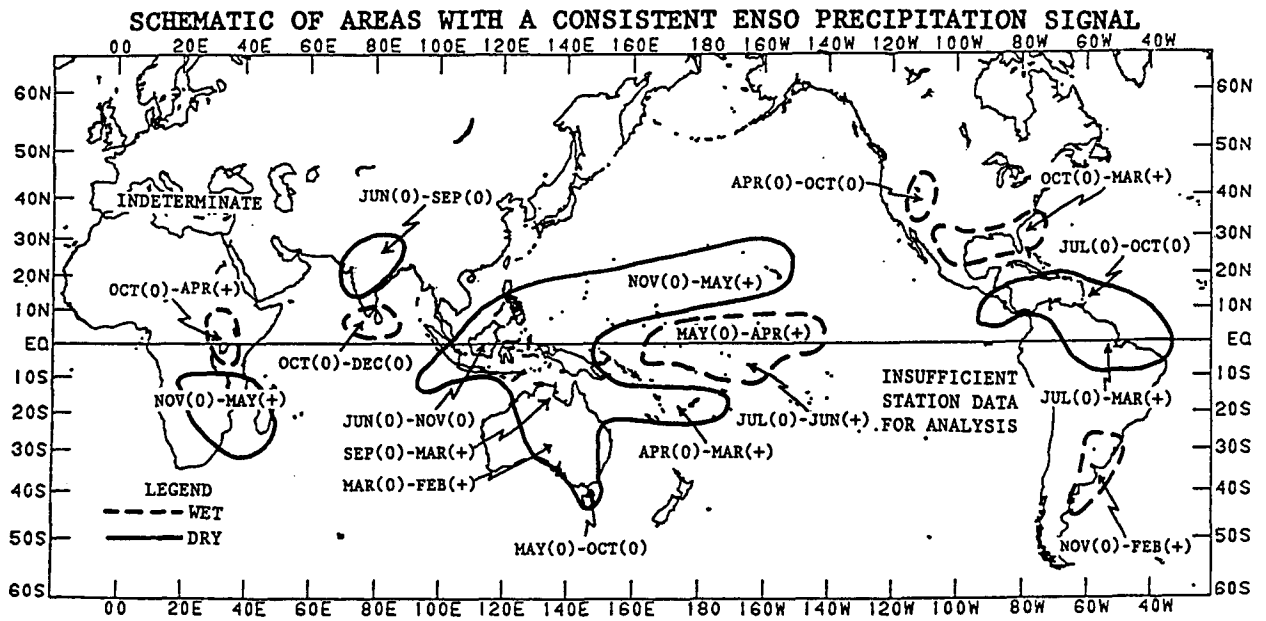

FIG. 21. Schematic representation of the principal ENSO-related precipitation based on the detailed analysis for the core regions. Regional maps should be consulted for details.

data are available. The most notable such omissions are likely along the west coast of South America and in the eastern Pacific.

Acknowledgments. We wish to thank E. Rasmusson for his suggestions and support during the course of this study. We also acknowledge the helpful comments and suggestions of V. Kousky and A. Barnston at the Climate Analysis Center and H. van den Dool of the Cooperative Institute for Climate Studies. Much of the data for this study were provided by R. Jenne, W. Spangler, and D. Shea of NCAR. We are also grateful for the very useful Australian data provided by M. Coughlan, Australian Bureau of Meteorology. J. Kopman provided valuable assistance in preparing the figures and K. Stevenson in preparing the text.

REFERENCES

Arkin, P. A., 1982: The relationship between interannual variability in the 200 mb tropical wind field and the Southern Oscillation. *Mon. Wea. Rev.*, **110**, 1393–1404.

Barnett, T. P., 1984: Interaction of the monsoon and Pacific trade wind system at interannual time scales. Part III: A partial anatomy of the Southern Oscillation. *Mon. Wea. Rev.*, **112**, 2388–2400.

Bergman, K. H., 1984: The climate of Autumn 1983—Featuring the conclusion of a major El Niño event. *Mon. Wea. Rev.*, **112**, 1441–1456.

Berlage, H. P., 1966: The Southern Oscillation and world weather. *Mededl. Verhandel.*, **88**, Kon. Ned. Meteor. Inst., 152 pp.

Chen, W. Y., 1983: The climate of Spring 1983—A season with persistent global scale anomalies associated with El Niño. *Mon. Wea. Rev.*, **111**, 2363–2384.

Dhonneur, G., 1974: Nouvelle approche des realites meteorologiques de l'Afrique occidentale et centrale. ASECNA, Universite de Dakar, Dakar, Senegal.

Douglas, A. V., and P. J. Englehart, 1981: On a statistical relationship between Autumn rainfall in the Central Equatorial Pacific and subsequent Winter precipitation in Florida. *Mon. Wea. Rev.*, **109**, 2377–2382.

Gordon, Neil D., 1986: The Southern Oscillation and New Zealand weather. *Mon. Wea. Rev.*, **114**, 371–387.

Hastenrath, S., 1978: On modes of tropical circulation and climate anomalies. *J. Atmos. Sci.*, **35**, 2222–2231.

——, and L. Heller, 1977: Dynamics of climatic hazards in northeast Brazil. *Quart. J. Roy. Meteor. Soc.*, **103**, 77–92.

——, and P. J. Lamb, 1977: *Climate Atlas of the Tropical Atlantic and Eastern Pacific Oceans,* The University of Wisconsin Press, XV + 97 pp.

Horel, J. D., and J. M. Wallace, 1981: Planetary-scale phenomenon associated with the Southern Oscillation. *Mon. Wea. Rev.*, **109**, 813–829.

Hsu, C. F., and J. M. Wallace, 1976: The global distribution of the annual and semiannual cycles in precipitation. *Mon. Wea. Rev.*, **104**, 1093–1101.

Kousky, V. E., M. T. Kagano and I. F. A. Cavalcanti, 1984: A review of the Southern Oscillation: oceanic–atmospheric circulation changes and related rainfall anomalies. *Tellus*, **36A**, 490–502.

Lamb, P. J., 1982: Persistence of subsaharan drought. *Nature*, **299**, 46–49.

Lau, K.-M., and P. H. Chan, 1983: Short-term variability and atmospheric teleconnections from satellite-observed outgoing longwave radiation. Part I: Simultaneous relationships. *J. Atmos. Sci.*, **40**, 2735–2750.

Lough, J. M., 1986: Tropical Atlantic sea surface temperatures and rainfall variations in Subsaharan Africa. *Mon. Wea. Rev.*, **114**, 561–570.

McBride, J. L., and N. Nicholls, 1983: Seasonal relationships between Australian rainfall and the Southern Oscillation. *Mon. Wea. Rev.*, **111**, 1998–2004.

Meisner, B. N., 1976: A study of Hawaiian and Line Island rainfall. *Rep. UHMET 76-4,* Dept. Meteor., University of Hawaii, Honolulu, 82 pp.

Nicholson, S. E., 1979: Revised rainfall series for the West African Subtropics. *Mon. Wea. Rev.*, **107**, 620–623.

——, 1985: Sub-Saharan rainfall 1981–1984. *J. Climate Appl. Meteor.*, **24**, 1388–1391.

Quiroz, R. S., 1983a: Relationships among stratospheric and tropospheric zonal flows and the Southern Oscillation. *Mon. Wea. Rev.*, **111,** 143–154.

——, 1983b: The climate of the "El Niño" winter of 1982–83—A season of extraordinary climatic anomalies. *Mon. Wea. Rev.*, **111,** 1685–1706.

Rasmusson, E. M., and T. H. Carpenter, 1982: Variations in tropical sea surface temperature and surface wind fields associated with the Southern Oscillation/El Niño. *Mon. Wea. Rev.*, **111,** 517–528.

——, and ——, 1983: The relationship between eastern equatorial Pacific sea surface temperatures and rainfall over India and Sri Lanka. *Mon. Wea. Rev.*, **111,** 517–528.

——, and J. M. Wallace, 1983: Meteorological aspects of the El Niño/Southern Oscillation. *Science,* **222,** 1195–1202.

Ropelewski, C. F., 1984: The climate of summer 1983—A season of contrasts and extremes. *Mon. Wea. Rev.*, **112,** 591–609.

——, 1986: North American precipitation patterns during the winter and spring of 1982–83 in comparison to the typical El Niño/Southern Oscillation (ENSO) response. *Proc. of the First WMO workshop on the diagnosis and prediction of monthly and seasonal atmospheric variations over the globe, College Park, MD, 29 July–2 August, 1985. Technical Document WMO/TD NO 87,* 191–200. [Available from the World Meteorological Organization, 41 Giuseppe-Motta, Case postale No. 5, CH-1211, Geneva 20, Switzerland.]

——, and M. S. Halpert, 1986: North American precipitation and temperature patterns associated with the El Niño Southern–Oscillation (ENSO). *Mon. Wea. Rev.*, **114,** 2352–2362.

——, J. E. Janowiak and M. S. Halpert, 1985: The analysis and display of real time surface climate data. *Mon. Wea. Rev.*, **113,** 1101–1106.

Shukla, J., and D. A. Paolino, 1983: The Southern Oscillation and long range forecasting of the summer monsoon rainfall over India. *Mon. Wea. Rev.*, **111,** 1830–1837.

Stoeckenius, T., 1981: Interannual variations of tropical precipitation patterns. *Mon. Wea. Rev.*, **109,** 1233–1247.

van Loon, H., and R. Madden, 1981: The Southern Oscillation. Part I: Global associations with pressure and temperature in northern winter. *Mon. Wea. Rev.*, **109,** 1150–1162.

Walker, G. T., 1923: Correlation in seasonal variations of weather, VIII: A preliminary study of world weather. *Mem. Indian Meteor. Dept.*, **24,** 75–131.

——, 1924: Correlation in seasonal variations of weather, IX: A further study of world weather. *Mem. Indian Meteor. Dept.*, **24,** 275–332.

——, 1928: World Weather III. *Mem. Roy. Meteor. Soc.*, **2,** 97–104.

——, and E. W. Bliss, 1930: World Weather IV. *Mem. Roy. Meteor. Soc.*, **3,** 81–95.

——, and ——, 1932: World Weather V. *Mem. Roy. Meteor. Soc.*, **4,** 53–84.

——, and ——, 1937: World Weather VI. *Mem. Roy. Meteor. Soc.*, **4,** 119–139.